The effect of microstructure on mechanical properties of directionally solidified intermetallic Ti-46Al-8Nb alloy

J. Lapin*, Z. Gabalcová, O. Bajana

Institute of Materials and Machine Mechanics, Slovak Academy of Sciences, Račianska 75, 831 02 Bratislava, Slovak Republic

Received 24 March 2009, received in revised form 27 May 2009, accepted 28 May 2009

Abstract

The effect of microstructure on mechanical properties of directionally solidified (DS) intermetallic Ti-46Al-8Nb (at.%) alloy was studied. After directional solidification at constant growth rates V ranging from 5.56×10^{-6} to 1.18×10^{-4} m s^{-1} and constant temperature gradients in liquid at the solid liquid interface G_L from 3.5×10^3 to 8×10^3 K m^{-1}, the DS samples contain several columnar grains aligned in a direction parallel or nearly parallel to the growth direction. The microstructure within the columnar grains is fully lamellar consisting of $\alpha_2(Ti_3Al) + \gamma(TiAl)$ lamellae. Mean α_2-α_2 interlamellar spacing λ decreases with increasing growth rate V and increasing cooling rate. Room temperature Vickers microhardness HV_m and compressive yield stress σ_y at 700 ℃ increase with decreasing interlamellar spacing λ according to Hall-Petch relationship. High-temperature compressive yield stress depends on an angle Θ between lamellar boundaries and loading axis. Maximum values of the yield stress are measured at $\Theta = 90°$ and minimum values at Θ ranging from 30° to 60°. Columnar grain structure leading to a high anisotropy of mechanical properties can be transformed to fine equiaxed grains with convoluted type of $\alpha_2 + \gamma$ microstructure by appropriate heat treatments. Compressive yield stress of the specimens with equiaxed grain structure continuously decreases with increasing test temperature. A simple relationship is proposed for a prediction of the compressive yield stress at temperatures ranging from 20 to 900 ℃.

K e y w o r d s: titanium aluminides, TiAl, crystal growth, heat treatments, phase transformations, microstructure, mechanical properties

1. Introduction

TiAl-based alloys represent an important class of high-temperature structural materials providing a unique set of physical and mechanical properties that can lead to substantial payoffs in the automotive industry, industrial gas turbines and aircraft engines [1–9]. Due to low density, high specific strength, high Young's modulus retention and oxidation resistance at high temperatures, TiAl-based alloys can be considered as good alternatives to currently used Ni-based alloys [10–13] and due to superior high-temperature mechanical properties can replace classical Ti-based alloys [14] or iron aluminides [15–18] at temperatures higher than about 600 ℃. Among various processing techniques, precise casting is very promising technology for production of complex shaped components [19]. However, casting of large components such as gas turbine blades leads to highly inhomogeneous microstructures composed of columnar and equiaxed grains [20]. Microstructure gradient results in variation and high anisotropy of mechanical properties of large cast blades [21]. As shown recently by Lapin and Gabalcová [8], refinement of columnar grain structure by post-solidification heat treatments through massive transformations depends significantly on the oxygen content and applied cooling rates. Frequently, some columnar grains can be preserved in the cast samples after the heat treatments, which leads to a high anisotropy of mechanical properties. Since growth of the columnar grains cannot be fully avoided by an appropriate modification of solidification conditions during casting of many large TiAl-based components, it is of large industrial importance to study the effect

*Corresponding author: tel.: +421 2 49268290; fax: +421 2 44253301; e-mail address: ummslapi@savba.sk

of columnar grains on local mechanical properties.

The purpose of this paper is to study the effect of microstructure on mechanical properties of directionally solidified (DS) intermetallic Ti-46Al-8Nb (at.%) alloy with columnar grain structure. In addition, the effect of columnar grain refinement achieved by post-solidification heat treatment on temperature dependence of yield stress is studied and discussed. The studied TiAl-based alloy has been selected as a potential material for the investment casting of low-pressure turbine blades of aircraft engines and industrial gas turbines within the European integrated project IMPRESS [22]. In this alloy, the addition of 8 at.% of Nb improves high oxidation resistance and 46 at.% of Al guarantees grain refinement of the as-cast microstructures during heat treatments [8, 23].

2. Experimental procedure

The intermetallic alloy with the chemical composition Ti-46Al-8Nb (at.%) and initial oxygen content of 500 wtppm was supplied in the form of vacuum arc re-melted cylindrical ingot with a diameter of 220 mm and a length of 60 mm. The ingot was cut to smaller blocks using electro spark machining and lathe machined to rods with a diameter of 8 and 15 mm and length of 120 mm. The cylindrical rods were put in dense cylindrical Y_2O_3 moulds (purity of 99.5 %) with a diameter of 8/12 mm and 15/20 mm (inside/outside diameter) and length of 130 mm and directionally solidified under argon atmosphere in a modified Bridgman-type apparatus described elsewhere [24]. Directional solidification of the samples with a diameter of 8 mm was performed at five constant growth rates V ranging from 5.56×10^{-6} to 1.18×10^{-4} m s^{-1} and three constant temperature gradients in liquid at the solid/liquid interface G_L of 3.5×10^3, 5×10^3 and 8×10^3 K m^{-1}. The samples with a diameter of 15 mm were directionally solidified at $V = 1.18 \times 10^{-4}$ m s^{-1} and $G_L = 6.5 \times 10^3$ K m^{-1}.

The DS samples with a diameter of 8 mm were solution annealed at a temperature of 1360 ℃ for 1 h in a dynamic argon atmosphere and subsequently cooled to room temperature at a rate of 50 K s^{-1}. The heat treatment was accomplished by stabilization annealing at 950 ℃ for 12 h in argon. The DS samples with a diameter of 15 mm were solution annealed at 1400 ℃ for 18 h and then cooled at a rate of 0.44 K s^{-1} in the resistance furnace under argon atmosphere. Cooling rates for heat treated samples were measured using computer data acquisition system with Pt-PtRh10 thermocouple placed in a sample hole with a diameter of 2.5 mm and length of 2 mm drilled specially for cooling rate measurements.

Vickers microhardness measurements were performed on longitudinal sections of DS samples at a load of 0.42 N. The loading time was 10 s. Cylindrical compression specimens with a diameter of 6 mm and length of 9 mm were lathe-machined from DS and heat-treated samples with a diameter of 8 mm. These specimens (5 specimens for each regime) were used to evaluate the effect of temperature on compressive yield stress. Rectangular compression specimens with dimensions of $3 \times 3 \times 4.5$ mm^3 were cut from the DS and heat-treated samples with a diameter of 15 mm by electric discharge machining. Each compression specimen was positioned within individual grain to achieve various angles between lamellar boundaries and the compressive loading axis ranging from 0° to 90°. Compression tests were performed at temperatures ranging from 20 ℃ to 900 ℃ and an initial strain rate of 1×10^{-4} s^{-1} in air using a screw driven universal testing machine Zwick. The compression offset yield stress was measured at 0.2 % plastic strain.

Microstructural analysis was performed by light optical microscopy (OM). OM samples were prepared using standard metallographic techniques and etched in a reagent of 50 ml H_2O, 3 ml HNO_3 and 1.5 ml HF. Quantitative metallographic analysis was performed on digitalized micrographs using a computerized image analyser.

3. Results and discussion

3.1. Formation of lamellar structure during directional solidification

The microstructure of DS samples with a diameter of 8 mm consisted of columnar dendritic grains (5–6) aligned in a direction parallel or nearly parallel to the growth direction, as shown in Fig. 1. The microstructure within the columnar grains is lamellar consisting of well-aligned γ(TiAl) and α_2(Ti_3Al) lamellae, as seen in Fig. 2. The average volume fraction of α_2-lamellae was measured to be (17.6 ± 1.1) vol.%. As shown recently by Gabalcová and Lapin [9], the studied Ti-46Al-8Nb (at.%) alloy solidifies

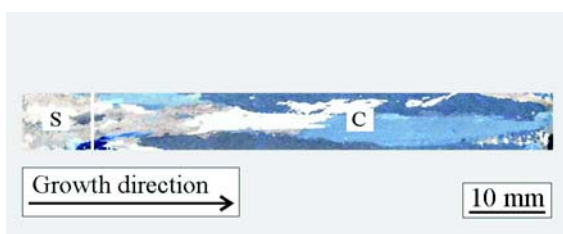

Fig. 1. Optical micrograph showing DS sample with columnar grain structure prepared at $V = 2.78 \times 10^{-5}$ m s^{-1} and $G_L = 3.5 \times 10^3$ K m^{-1}. S – non-melted part of the sample, C – columnar grain structure.

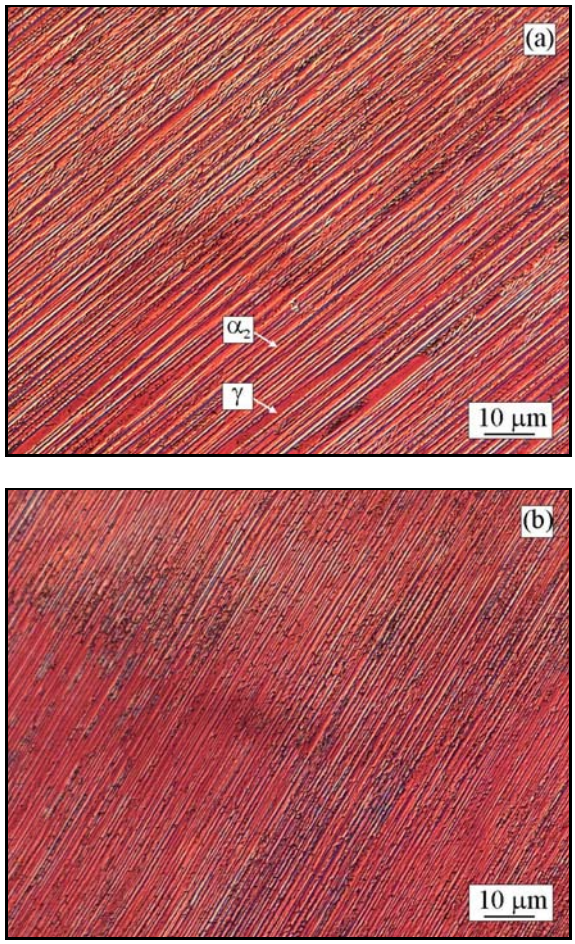

Fig. 2. Optical micrographs showing lamellar $\alpha_2+\gamma$ microstructure of DS samples prepared at $G_L = 5 \times 10^3$ K m^{-1}: (a) $V = 5.56 \times 10^{-6}$ m s^{-1}; (b) $V = 1.18 \times 10^{-4}$ m s^{-1}.

through β-phase (Ti-based solid solution with cubic crystal structure) without any evidence of peritectic reaction. Since the preferred growth direction of the β-dendrites is close [001] crystallographic direction, {011} planes grow with an angle of 0° or 45° to the growth direction. When the β-phase transforms to α-phase (Ti-based solid solution with hexagonal crystal structure), the crystallographic orientation relationship $(110)_\beta \| (0001)_\alpha$ is maintained between coexisting phases [25]. Since the γ-lamellae precipitate from the parent α phase following Blackburn crystallographic orientation relationships of $(0001)_\alpha \| \{111\}_\gamma$ and $\langle 11\bar{2}0\rangle_\alpha \| \langle 1\bar{1}0]_\gamma$ [26], it makes the lamellar boundary inclined at an angle of 0° or 45° to the growth direction. As shown by Denquin and Naka [27], formation of lamellar structure results from the precipitation of γ-lamellae in either a disordered α- or an ordered α_2-matrix. During continuous cooling from the α-phase field, the formation of γ-lamellae starts in the $\alpha + \gamma$ phase field and is finalized in $\alpha_2 + \gamma$ phase field. The whole sequence of the lamellar structure formation involves three stages: (i) change of the crystal structure from h.c.p. to f.c.c. by propagation of Shockley partial dislocations in the hexagonal matrix; (ii) a chemical composition change through atom transfer by a combined shear and diffusion process, and (iii) an ordering reaction of the f.c.c. structure leading to the final $L1_0$ γ-phase.

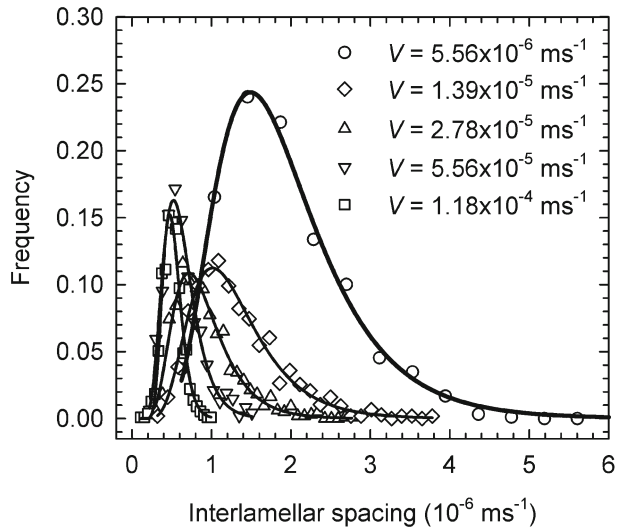

Fig. 3. Log-normal distribution curves of interlamellar α_2-α_2 spacing measured in DS samples prepared at $G_L = 5 \times 10^3$ K m^{-1}. The applied growth rates V are indicated in the figure.

Figures 2a and 2b indicate that increase of the growth rate refines $\alpha_2 + \gamma$ lamellar microstructure. The measured statistical data of α_2-α_2 interlamellar spacing λ_m (about 1000 measurements for each growth regime) were fitted by a log-normal distribution function $\Phi(\lambda_m)$ in the form

$$\Phi(\lambda_m) = \frac{1}{\sigma_m \sqrt{2\pi}} \exp\left[-\frac{(\ln \lambda_m - \ln \lambda)^2}{2\sigma_m^2}\right], \qquad (1)$$

where λ is the mean value function and σ_m is the parameter of log-normal distribution. Figure 3 shows the typical examples of log-normal distribution curves resulting from the statistical evaluation of interlamellar spacing at five growth rates and a constant temperature gradient of $G_L = 5 \times 10^3$ K m^{-1}. Similar log-normal distribution curves were determined for DS samples prepared at $G_L = 3.5 \times 10^3$ K m^{-1} and $G_L = 8 \times 10^3$ K m^{-1}. Figure 4 shows variation of the mean interlamellar spacing λ with the growth rate V at three temperature gradients G_L. It is clear that λ decreases proportionally with increasing V according to relationship

$$\lambda = K_1 V^{-a}, \qquad (2)$$

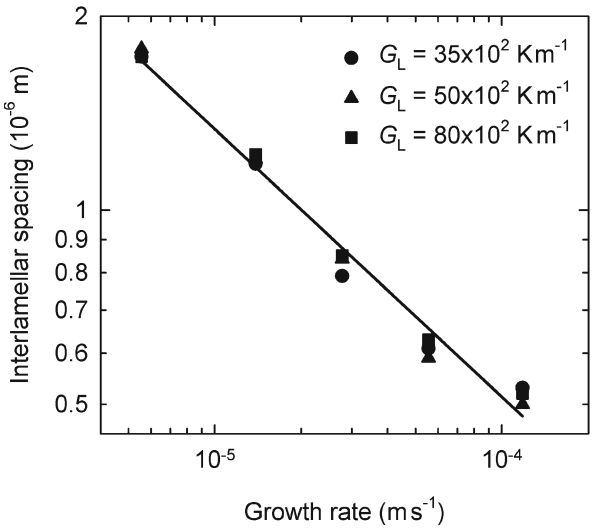

Fig. 4. Dependence of mean α_2-α_2 interlamellar spacing on growth rate. The applied temperature gradients G_L are indicated in the figure.

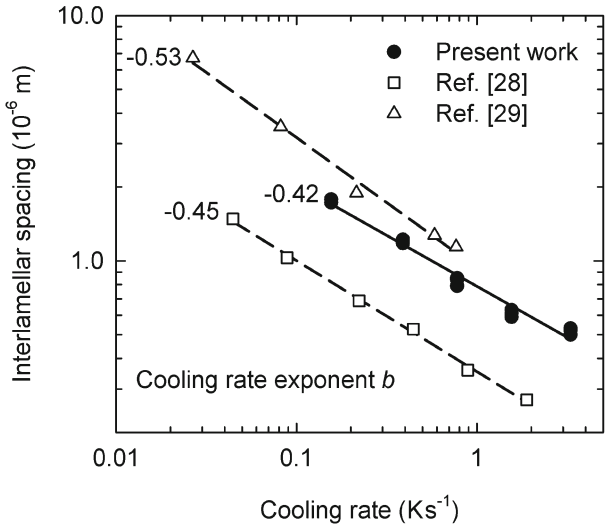

Fig. 5. Dependence of mean α_2-α_2 interlamellar spacing on cooling rate.

where K_1 is a material constant and a is the growth rate exponent. The statistical analysis confirms that λ is independent from G_L. Using regression analysis of all data shown in Fig. 4, the dependence of λ on V can be expressed in the form

$$\lambda = 1.12 \times 10^{-8} V^{-0.42}. \tag{3}$$

The correlation coefficient of this fit is $r^2 = 0.98$. Lapin et al. [24, 28] and Perdrix et al. [29] showed that interlamellar spacing λ depends on cooling rate $\dot{v}$ defined as

$$\dot{v} = V G_S, \tag{4}$$

where G_S is the temperature gradient in the solid. The temperature gradient G_S was measured during directional solidification by the procedure described elsewhere by Gabalcová and Lapin [9] at temperatures ranging from 1330 to 1170 ℃ that correspond to precipitation of γ-lamellae from the α-matrix [30]. The measured value of $G_S = (280 \pm 8) \times 10^2$ K m^{-1} was found to be independent from the applied growth rates and temperature gradients G_L. Figure 5 shows dependence of interlamellar spacing λ on cooling rate $\dot{v}$. Interlamellar spacing λ decreases proportionally with increasing $\dot{v}$ according to relationship in the form

$$\lambda = K_2 \dot{v}^{-b}, \tag{5}$$

where K_2 is a material constant and b is the cooling rate exponent. Using regression analysis, the dependence of the interlamellar spacing on the growth rate can be expressed in the form

$$\lambda = 7.87 \times 10^{-7} \dot{v}^{-0.42}. \tag{6}$$

The correlation coefficient of this fit is $r^2 = 0.98$. The cooling rate exponent of $b = 0.42$ is comparable with that of 0.45 measured by Lapin [28] for DS Ti-46Al--2W-0.5Si (at.%) alloy and is lower than that of 0.53 reported by Perdrix et al. [29] for a binary Ti-48Al (at.%) alloy, as seen in Fig. 5.

3.2. Effect of interlamellar spacing on microhardness and yield stress

Figure 6 shows dependence of the Vickers microhardness HV_m on the reciprocal square root of α_2-α_2 interlamellar spacing λ for all DS samples. Vickers microhardness decreases with increasing λ. The measured microhardness values HV_m can be fitted to a Hall-Petch type relationship in the form

$$HV_m = HV_o + k_{HV} \frac{1}{\sqrt{\lambda}}, \tag{7}$$

where HV_o and k_{HV} are material constants. Linear regression analysis of the experimental data yields an equation for the microhardness HV_m in the form

$$HV_m = 3.04 + 1.34 \times 10^{-3} \frac{1}{\sqrt{\lambda}}, \tag{8}$$

where dimension of λ is given in m. The correlation coefficient of this fit is $r^2 = 0.99$. The measured slope of the regression line of $k_{HV} = 1.34 \times 10^{-3}$ GPa m$^{0.5}$ is significantly lower than that of 2.7×10^{-3} GPa m$^{0.5}$ measured by Lapin et al. [31] for DS Ti-46Al-2W-

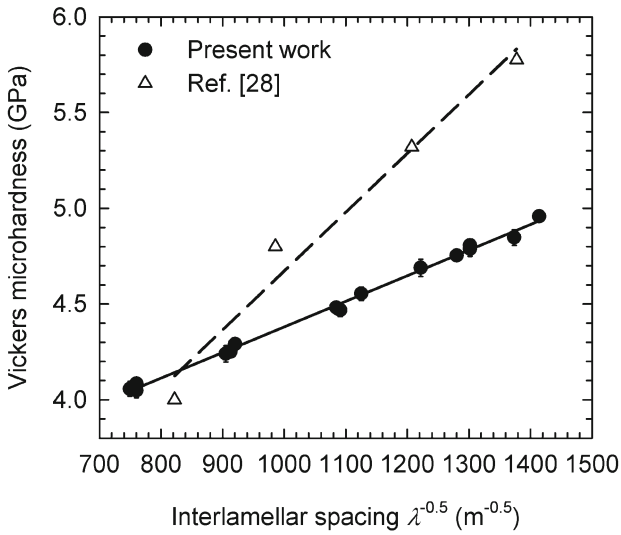

Fig. 6. Dependence of Vickers microhardness on the reciprocal square root of interlamellar spacing λ.

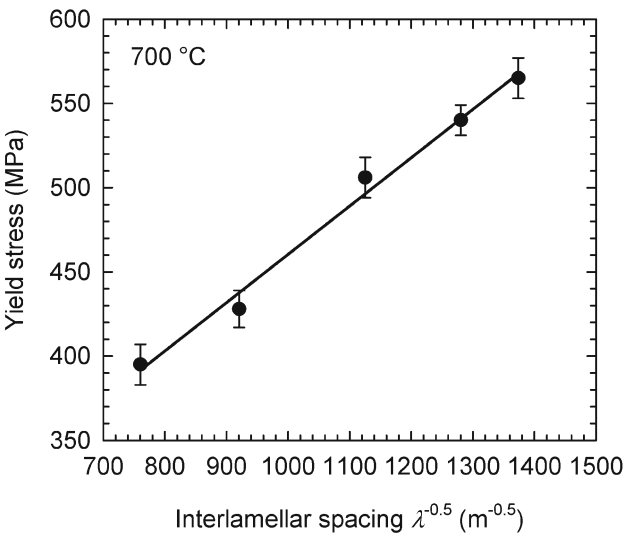

Fig. 7. Dependence of yield stress on the reciprocal square root of interlamellar spacing λ at 700 °C.

-0.5Si (at.%) alloy. The reason of significantly higher average values of HV_m and k_{HV} measured in reference DS Ti-46Al-2W-0.5Si (at.%) alloy in comparison with those of the studied Ti-46Al-8Nb (at.%) alloy is twofold: (i) higher volume fraction of α_2 lamellae (about 40 vol.% in the reference alloy) leading to numerous strong α_2/γ interfaces and (ii) solution strengthening and stabilization of the α_2-phase by oxygen resulting from contamination of the reference alloy due to reaction of the melt with alumina moulds during directional solidification [32].

Several authors [28, 33–36] have described the strengthening effect of lamellae by a Hall-Petch type relationship in the form

$$\sigma_y = \sigma_o + k_y \frac{1}{\sqrt{\lambda}}, \tag{9}$$

where σ_y is the yield stress, σ_o is the stress corresponding to the lattice resistance to dislocation slip in the γ-phase and k_y is a parameter which is related to the critical stress necessary to generate a dislocation in the α_2-lamella. Figure 7 shows dependence of average yield stress on the reciprocal square root of interlamellar spacing λ at a temperature of 700 °C. It should be noted that the compression specimens (5 specimens for each regime) with a diameter of 6 mm contained several columnar grains with a predominant lamellar orientation ranging from 38° to 58° to the compressive loading axis. Linear regression analysis of the experimental data yields an equation for the yield stress in the form

$$\sigma_y = 173.7 + 0.29 \frac{1}{\sqrt{\lambda}}, \tag{10}$$

where dimension of λ is given in m. The correlation coefficient of this fit is $r^2 = 0.98$. The parameter $k_y = 0.29\,\mathrm{MPa\,m^{0.5}}$ corresponds to that of $0.29\,\mathrm{MPa\,m^{0.5}}$ measured by Maruyama et al. [35] and is comparable with that of $0.27\,\mathrm{MPa\,m^{0.5}}$ determined by Umakoshi and Nakano [36] for the compression specimens with lamellar orientation of 45° to loading axis. On the contrary, our value is higher than those of $0.078\,\mathrm{MPa\,m^{0.5}}$ reported by Perdrix et al. [29], $0.1\,\mathrm{MPa\,m^{0.5}}$ of Dimiduk et al. [33] and lower than those of 0.50 and $0.41\,\mathrm{MPa\,m^{0.5}}$ determined by Umakoshi and Nakano [36] for the compression specimens with lamellar orientation of 90° and 0° to loading axis, respectively.

The aligned α_2-lamellae are strong barriers to dislocation motion and dislocations generated in the γ-phase pile-up at the α_2/γ interfaces [37]. According to the traditional pile-up model of edge dislocations at a single barrier, the Hall-Petch slope k_y is given by [33, 35]

$$k_y = M\sqrt{\frac{Gb\tau^*}{1-\nu}}, \tag{11}$$

where M is the Taylor factor ($M = 3$), G is the shear modulus (60 GPa) [37], b is the length of Burgers vector (0.284 nm), τ^* is the shear stress of the barrier to dislocation motion and ν is the Poisson's ratio (0.234). Taking Eq. (11) and experimentally determined value of $k_y = 0.29\,\mathrm{MPa\,m^{0.5}}$, one can calculate shear stress necessary for dislocation to overcome the α_2/γ interlamellar interfaces of $\tau^* = 420\,\mathrm{MPa}$. Critical minimum interlamellar spacing λ^*, which is still effective to increase the yield stress, can be calculated according to

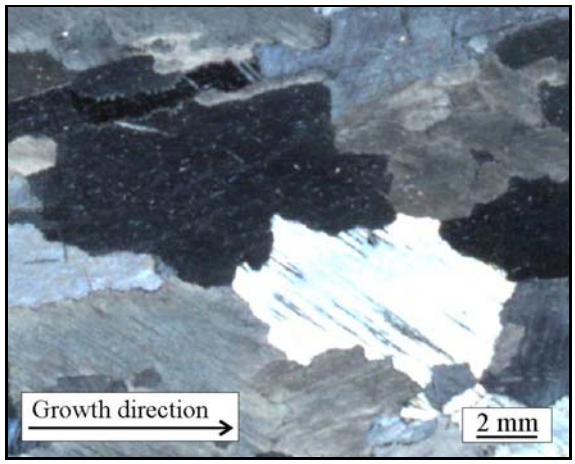

Fig. 8. The typical grain structure of DS solidified samples with a diameter of 15 mm after annealing at 1400 °C for 18 h.

equation in the form [35]

$$\lambda^* = \frac{Gb}{(1-\nu)\,\tau^*}. \qquad (12)$$

Taking Eq. (12), one can calculate a critical interlamellar spacing of $\lambda^* = 5.3 \times 10^{-8}$ m. Interlamellar spacings $\lambda < \lambda^*$ will be not more effective to increase further the yield stress of the studied alloy according to Eq. (10).

3.3. Effect of lamellar orientation on yield stress

Figure 8 shows the typical grain structure of DS samples with a diameter of 15 mm after annealing at 1400 °C for 18 h. The microstructure of the grains is fully lamellar consisting from $\alpha_2 + \gamma$ lamellae with a mean α_2-α_2 interlamellar spacing of $\lambda = 620$ nm. Rectangular compression specimens with dimensions of $3 \times 3 \times 4.5$ mm^3 were positioned within these grains to achieve various lamellar boundary orientations ranging from 0° to 90° to the compression loading axis. Figure 9 shows the typical $\alpha_2 + \gamma$ lamellar microstructure of the compression specimens. After achieving 0.2 % offset yield stress the compression tests were interrupted and the specimens were subjected to metallographic analysis. Successive metallographic sections (3–4 for each specimen) revealed that in spite of selecting single grain with required lamellar boundary orientation shown in Fig. 9a, each compression specimen contained one or two minor grains with random lamellar orientations occupying up to 20 vol.%, as illustrated in Fig. 9b.

Figure 10 shows dependence of yield stress on angle Θ between loading axis and lamellar boundaries of the main grain. The yield stress depends strongly on the

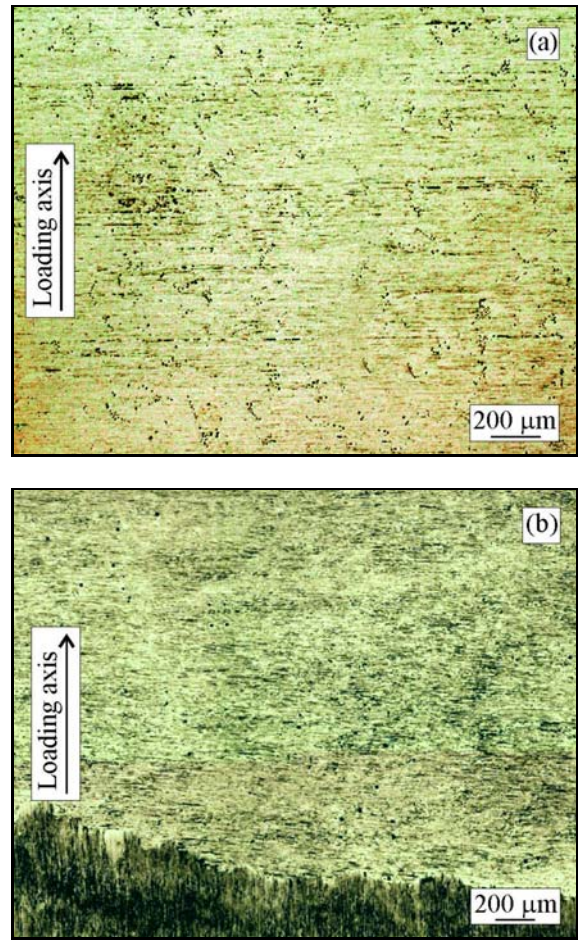

Fig. 9. Optical micrographs showing the typical $\alpha_2 + \gamma$ lamellar microstructure of compression specimens: (a) orientation of lamellar boundaries at an angle of 90° to the loading axis in the main grain; (b) orientation of lamellar boundaries at an angle of 90° and 0° to the loading axis in the main and minor grain, respectively.

angle Θ and decreases with increasing test temperature. The highest values of the yield stress are measured for the specimens with $\Theta = 90°$. When Θ is from the range 30°–60°, the yield stress is significantly lower and achieves only of about 47 % of the maximum values measured at $\Theta = 90°$. The evolution of the yield stress with the angle Θ is similar to that reported by Inui et al. [38] for polysynthetically twinned Ti-49.3Al (at.%) crystals or those of Ti-48.4Al-0.6V and Ti-48.4Al-0.6Zr (at.%) crystals measured by Yao et al. [39] in compression at room temperature. Previous authors [38, 39] observed no particular difference between yield stress measured in tension and compression. As shown by Inui et al. [38], one of the two major deformation modes in the γ-phase, i.e. the major constituent phase of polysynthetically twinned crystals, is twinning of the $\{111\}\langle 11\bar{2}]$ type and slip along $\langle 11\bar{2}]$ direction. Which of the two major deformation modes is operative depends on crystal orientation. In

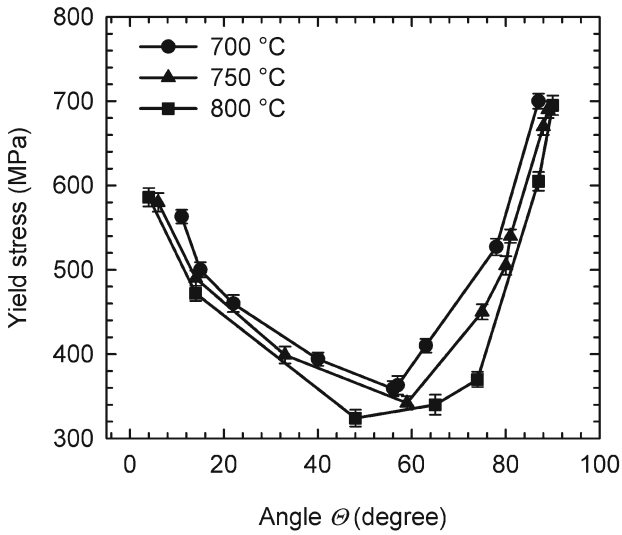

Fig. 10. Dependence of compressive yield stress on an angle Θ between loading axis and lamellar boundaries of the main grain. The test temperatures are indicated in the figure.

general, slip along $\langle 11\bar{2}]$ direction is activated in domains in which deformation twinning cannot occur. Then, the domains, which deform by twinning in tension, deform by slip in compression and vice versa. In other words, when loading mode is changed, twinning and slip exchange domains where they operate, but the deformation behaviour of the crystal as a whole is not changed.

3.4. Effect of columnar grain refinement on yield stress

Figure 11 shows influence of solution annealing at 1360 ℃ (single α-phase field) for 1 h followed by free air cooling (AC) on the microstructure of the DS samples with a diameter of 8 mm containing 1400 wtppm of oxygen. During the heat treatment the columnar grain structure fully transformed to equiaxed grains due to transformation of α-phase to massive γ_M. After AC the samples contain three microstructurally different regions, which could be clearly distinguished and quantified by means of optical microscopy: (i) massive γ_M (72 vol.%), (ii) retained α_R (25 vol.%) and (iii) lamellar $\alpha_2 + \gamma$ microstructure (3 vol.%), as seen in Fig. 11a. As shown by several authors [8, 38, 39], massive transformation of the α-phase to massive γ_M results in fine grain structure due to formation of many small subgrains by successive twinning of growing massively transformed γ_M. Huang et al. [23, 40] have shown that the subgrains formed by twinning have no simple crystallographic orientation relation with the parent α-phase and the loss of any orientation relationship is caused

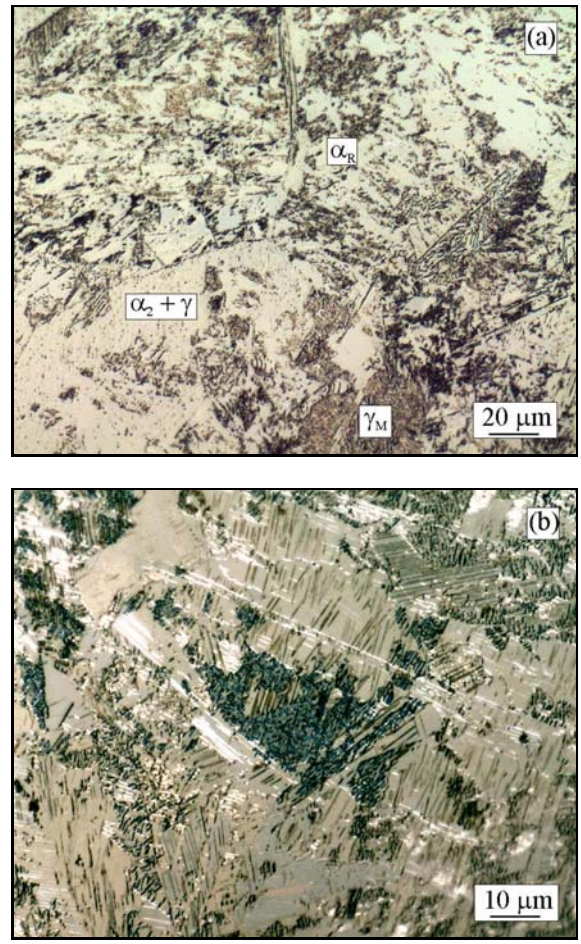

Fig. 11. The typical microstructure of DS samples with a diameter of 8 mm after the heat treatment applied for columnar grain refinement: (a) solution annealing at 1360 ℃ for 1 h and free air cooling to room temperature; (b) convoluted type of microstructure after stabilization annealing at 950 ℃ for 20 h.

also by formation of high angle boundaries between the growing regions of massive γ_M. On the other hand, Dey et al. [41] have confirmed Blackburn crystallographic orientation relationship, i.e. $(0002)_\alpha \parallel (111)_\gamma$ and $[11\bar{2}0]_\alpha \parallel [1\bar{1}0]_\gamma$, between massive γ_M grains and one of the two parent α grains during nucleation and growth of the massive γ_M. In spite of a large discrepancy among experimental studies concerning crystallographic orientation relationships between the parent α-phase and massive γ_M grains, there are no doubts that the α-α grain boundaries are preferential nucleation sites for massive γ_M in many TiAl-based alloys. Huang et al. [42] and Lapin and Gabalcová [8] have observed that the local oxygen level increases at grain boundaries during cooling at slow rates and such higher oxygen content stabilizes the α-phase so that massive transformation can be suppressed locally.

Figure 11b shows the typical microstructure of compression specimens after stabilization annealing

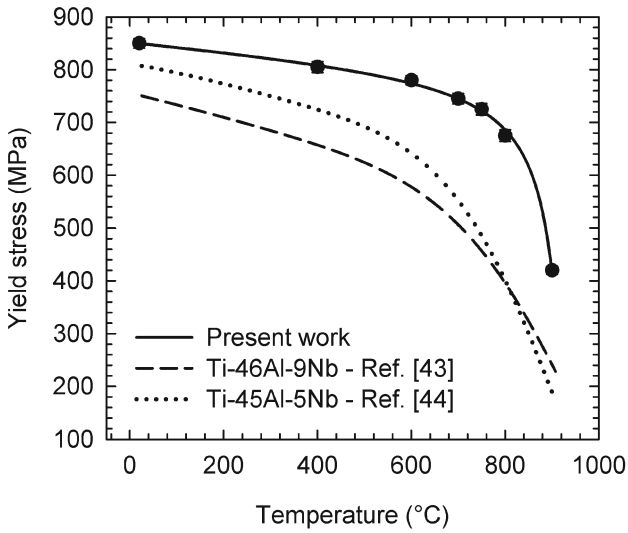

Fig. 12. Temperature dependence of compressive yield stress for DS samples with a diameter of 8 mm after heat treatment applied for the columnar grain refinement.

at 950 °C for 12 h. During stabilization annealing the α-phase precipitates from γ_M and forms convoluted type of $\alpha_2 + \gamma$ microstructure. Statistically determined mean and maximum grain size (about 800 measurements) from log-normal distribution curve of 8.5 μm and 165 μm, respectively, clearly indicates effectiveness of the applied heat treatment on refinement of columnar grains with an average diameter of about 2100 μm. Figure 12 shows dependence of 0.2 % offset yield stress on temperature. The yield stress decreases continuously with increasing temperature T (in °C). The data shown in Fig. 12 represent average values from five compressive specimens with loading axis parallel to the ingot axis tested at each temperature. Non-linear regression analysis of the data shown in Fig. 12 yields an equation for the yield stress σ_y in the form

$$\sigma_y = \frac{851.61 - 0.92T}{1 - 9.68 \times 10^{-4}T - 8.99 \times 10^{-8}T^2}. \qquad (13)$$

The correlation coefficient of this fit is $r^2 = 0.98$. Equation (13) can be used as a simple prediction tool of the yield stress for temperatures ranging from 20 to 900 °C. The measured compressive yield stress over the studied temperature range is higher than those reported by Gerling et al. [43, 44] for Ti-46Al-9Nb and Ti-45Al-5Nb (at.%) sheets prepared by powder metallurgical processing.

4. Conclusions

The investigation of the effect of microstructure on mechanical properties of DS Ti-46Al-8Nb (at.%) alloy suggests the following conclusions:

1. During directional solidification at constant growth rates V ranging from 5.56×10^{-6} to 1.18×10^{-4} m s^{-1} and constant temperature gradient G_L ranging from 3.5×10^3 to 8×10^3 K m^{-1} the mean α_2-α_2 interlamellar spacing λ depends on V and is independent from G_L. The interlamellar spacing decreases with increasing growth rate V and increasing cooling rate defined as $\dot{v} = G_S V$, where G_S is the temperature gradient in the solid.

2. Room-temperature Vickers microhardness HV_m and compressive yield stress σ_y at 700 °C increase with decreasing interlamellar spacing λ according to Hall-Petch relationships in the form $HV_m \propto 1/\sqrt{\lambda}$ and $\sigma_y \propto 1/\sqrt{\lambda}$, respectively.

3. High-temperature compressive yield stress depends on an angle Θ between lamellar boundaries of the main grain and loading axis. Maximum values of the yield stress are measured at $\Theta = 90°$ and minimum values at Θ ranging from 30° to 60°. The yield stress decreases with increasing temperature.

4. Columnar grain structure leading to a high anisotropy of mechanical properties can be transformed to fine equiaxed one with convoluted type of $\alpha_2 + \gamma$ microstructure by appropriate heat treatments. Compressive yield stress of the specimens with refined grain structure continuously decreases with increasing temperature. A simple relationship derived from experimental data was proposed for a prediction of the yield stress at temperatures ranging from 20 °C to 900 °C.

Acknowledgements

This work was financially supported by EU Integrated Project IMPRESS Intermetallic Materials Processing in Relation to Earth and Space Solidification under the contract No. NMP3-CT-2004-500635 and the Slovak Research and Development Agency under the contract APVV-0009-07.

References

[1] LORIA, E. A.: Intermetallics, *8*, 2000, p. 1339.
[2] TETSUI, T.: Mater. Sci. Eng. A, *329–331*, 2002, p. 582.
[3] WU, X.: Intermetallics, *14*, 2006, p. 1114.
[4] GEBAUER, K.: Intermetallics, *14*, 2006, p. 355.
[5] LASALMONIE, A.: Intermetallics, *14*, 2006, p. 1123.
[6] DIMIDUK, D. M.: Mater. Sci. Eng. A, *263*, 1999, p. 281.
[7] NODA, T.: Intermetallics, *6*, 1998, p. 709.
[8] LAPIN, J.—GABALCOVÁ, Z.: Kovove Mater., *46*, 2008, p. 185.
[9] GABALCOVÁ, Z.—LAPIN, J.: Kovove Mater., *45*, 2007, p. 231.
[10] SAJJADI, S. A.—NATEGH, S.—GUTHRIE, R. I. L.: Mater. Sci. Eng. A, *325*, 2002, p. 484.

[11] ZHAO, S.—XIE, X.—SMITH, G. D.—PATEL, S. J.: Mater. Sci. Eng. A, *355*, 2003, p. 96.
[12] HOU, J. S.—GUO, J. T.—ZHOU, L. Z.—YUAN, C.—YE, H. Q.: Mater. Sci. Eng. A, *374*, 2004, p. 327.
[13] CAI, D.—XIONG, L.—LIU, W.—SUN, G.—YAO, M: Mater. Charact., *58*, 2007, p. 941.
[14] EISENBARTH, E.—VELTEN, D.—MÜLLER, M.—THULL, R.—BREME, J.: Biomaterials, *25*, 2004, p. 5705.
[15] DEEVI, S. C.—SIKKA, V. K.: Intermetallics, *4*, 1996, p. 357.
[16] DEEVI, S. C.—SWINDEMAN, R. W.: Mater. Sci. Eng. A, *258*, 1998, p. 203.
[17] KRATOCHVÍL, P.—MÁLEK, P.—CIESLAR, M.—HANUS, P.—HAKL, J.—VLASÁK, T.: Intermetallics, *15*, 2007, p. 333.
[18] SCHNEIDER, A.—FALAT, L.—SAUTHOFF, G.—FROMMEYER, G.: Intermetallics, *13*, 2005, p. 1322.
[19] HARDING, R. A.: Kovove Mater., *42*, 2004, p. 225.
[20] LAPIN, J.—NAZMY, M.: Mater. Sci. Eng. A, *380*, 2004, p. 298.
[21] LAPIN, J.—KLIMOVÁ, A.: Kovove Mater., *41*, 2003, p. 1.
[22] JARVIS, D. J.—VOSS, D.: Mater. Sci. Eng. A, *413–414*, 2005, p. 583.
[23] HUANG, A.—HU, D.—WU, X.—LORETTO, M. H.: Intermetallics, *15*, 2007, p. 1147.
[24] LAPIN, J.—ONDRÚŠ, Ľ.—NAZMY, M.: Intermetallics, *10*, 2002, p. 1019.
[25] JUNG, I. S.—KIM, M. C.—LEE, J. H.—OH, M. H.—WEE, D. M.: Intermetallics, *7*, 1999, p. 1247.
[26] INUI, H.—NAKAMURA, A.—OH, M. H.—YAMAGUCHI, M.: Ultramicroscopy, *39*, 1991, p. 268.
[27] DENQUIN, A.—NAKA, S.: Acta Mater., *44*, 1996, p. 343.
[28] LAPIN, J.: J. Mater. Sci. Lett., *22*, 2003, p. 747.
[29] PERDRIX, F.—TRICHET, M. F.—BONNENTEIN, J. L.—CORNET, M.—BIGOT, J.: Intermetallics, *7*, 1999, p. 1323.
[30] WITUSIEWICZ, V. T.—BONDAR, A. A.—HECHT, U.—VELIKANOVA, T. Ya.: J. Alloys Compd., *472*, 2009, p. 133.
[31] LAPIN, J.—ONDRÚŠ, Ľ.—BAJANA, O.: Mater. Sci. Eng. A., *360*, 2003, p. 85.
[32] LAPIN, J.—ONDRÚŠ, Ľ.: Kovove Mater., *40*, 2002, p. 161.
[33] DIMIDUK, D. M.—HAZZLEDINE, P. M.—PARTHASARATHY, T. A.—SESHAGIRI, S.—MENDIRATTA, M. G.: Metall. Mater. Trans., *29A*, 1998, p. 37.
[34] PARTHASARATHY, T. A.—MENDIRATTA, M. G.—DIMIDUK, D. M.: Acta Mater., *46*, 1998, p. 4005.
[35] MARUYAMA, M.—YAMADA, N.—SATO, H.: Mater. Sci. Eng. A, *319–321*, 2001, p. 360.
[36] UMAKOSHI, Y.—NAKANO, T.: Acta Metall. Mater., *41*, 1993, p. 1155.
[37] LAPIN, J.: Intermetallics, *14*, 2006, p. 115.
[38] INUI, H.—OH, M.H.—NAKAMURA, A.—YAMAGUCHI, M.: Acta Metall. Mater., *40*, 1992, p. 3059.
[39] YAO, K. F.—INUI, H.—KISHIDA, K.—YAMAGUCHI, M.: Acta Metall. Mater., *43*, 1995, p. 1075.
[40] HUANG, A.—HU, D.—LORETTO, M. H.—WU, X.: Intermetallics, *17*, 2009, p. 285.
[41] DEY, S. R.—BOUZY, E.—HAZOTTE, A.: Intermetallics, *14*, 2006, p. 444.
[42] HUANG, A.—LORETTO, M. H.—HU, D.—LIU, K.—WU, X.: Intermetallics, *14*, 2006, p. 838.
[43] GERLING, R.—BARTELS, A.—CLEMENS, H.—KESTLER, H.—SCHIMANSKY, F. P.: Intermetallics, *12*, 2004, p. 275.
[44] GERLING, R.—SCHIMANSKY, F. P.—STARK, A.—BARTELS, A.—KESTLER, H.—CHA, L.—SCHEU, C.—CLEMENS, H.: Intermetallics, *16*, 2008, p. 689.